JOURNAL OF AIRCRAFT
Vol. 45, No. 4, July–August 2008

Role Identification of Yaw and Sway Motion in Helicopter Yaw Control Tasks

J. Ellerbroek,* O. Stroosma,† M. Mulder,‡ and M. M. van Paassen§
Delft University of Technology, 2629 HS Delft, The Netherlands

DOI: 10.2514/1.34513

A set of experiments has been conducted to investigate the relative effect of translational and rotational motion cues on pilot performance. Two helicopter yaw control tasks were performed on the SIMONA: a yaw capture task and a target-tracking task with simulated turbulence. The yaw capture task was a repetition of a task performed previously at two different simulator facilities. Shaping filters and added delays were used to match simulator characteristics with the previous experiments. In contrast to previous conclusions, results from the current study show more equal contributions of yaw and sway motion on performance and subjective simulator motion fidelity. Analyses of the different vestibular cues using multiloop pilot models, estimated from measurement data from the target-tracking task, also indicate comparable utilization of the yaw and sway motion cues.

Nomenclature

$A_{1,2}$	=	frequency sweep magnitudes
B_p	=	pilot effective leg damping
B_r	=	rudder pedal selected damping
$d_{a,b}$	=	filter denominator parameters
e	=	error signal $\psi_t - \psi$
F	=	frequency sweep signal
f_b	=	forcing function base frequency
$f^b_{x,\mathrm{ps}}$	=	longitudinal specific force at the pilot station
$f^b_{y,\mathrm{ps}}$	=	lateral specific force at the pilot station
H_{ah64}	=	Apache approximated dynamics
H_e	=	parametric visual path with simulator dynamics
$\hat{H}_e$	=	identified visual path
H_{nms}	=	neuromuscular system dynamics
H_{oto}	=	otolith dynamics
H_{p_e}	=	parametric visual path
H_{p_x}	=	parametric vestibular path
H_{scc}	=	semicircular canal dynamics
H_{shaping}	=	shaping filter
H_{SRS}	=	SIMONA Research Simulator approximated dynamics
$H_{\mathrm{srs},\psi}$	=	SIMONA Research Simulator yaw approximated dynamics
$H_{\mathrm{srs},v}$	=	SIMONA Research Simulator visual approximated dynamics
$H_{\mathrm{srs},y}$	=	SIMONA Research Simulator lateral approximated dynamics
H_{vis}	=	visual perception dynamics
H_{VMS}	=	vertical motion simulator describing function
$\tilde{H}_{\mathrm{SRS}}$	=	SIMONA Research Simulator measured dynamics
H_x	=	parametric vestibular path with simulator dynamics
$\hat{H}_x$	=	identified vestibular path
J	=	cost function
K	=	washout filter gain
K_v	=	visual perception gain
K_y	=	otolith perception gain
K_ψ	=	semicircular canal perception gain
k_p	=	pilot effective leg stiffness
k_r	=	rudder pedal selected stiffness
L	=	distance from pilot to helicopter center of gravity
m_p	=	pilot effective leg mass
m_r	=	rudder pedal selected mass
n	=	pilot model remnant
n	=	white noise
$\bar{n}$	=	mean SIMONA Research Simulator model remnant
n_w	=	pilot model remnant
$n_{a,b}$	=	shaping filter numerator parameters
p	=	probability that the null hypothesis is true
r	=	yaw angular rate
$\dot{r}$	=	yaw angular acceleration
S_{xx}	=	power spectral density
S_{xy}	=	cross-spectral density
s	=	Laplace operator
u	=	identified model output
X_b	=	aircraft body X axis
x	=	state signal ψ
Y_b	=	aircraft body Y axis
$\ddot{y}$	=	lateral acceleration
δ_d	=	disturbance forcing function
δ_p	=	pedal input
ζ	=	damping factor
ζ_{nm}	=	neuromuscular damping factor
θ	=	optimization parameter vector
ρ	=	coherence function
σ	=	standard deviation
σ_n	=	SIMONA Research Simulator remnant standard deviation
$\tau_{1,2}$	=	semicircular canal lag terms
τ_3	=	otolith lag term
τ_{d_ψ}	=	canal perception delay
τ_{d_v}	=	visual perception delay
τ_{d_y}	=	otolith perception delay
τ_L	=	canal neural lead term
τ_{L_v}	=	visual path lead term
τ_n	=	otolith neural lead term
ϕ	=	frequency sweep phase angle

Presented as Paper 6800 at the AIAA Modeling and Simulation Technologies Conference and Exhibit, Hilton Head, SC, 20–23 August 2007; received 10 September 2007; revision received 26 November 2007; accepted for publication 26 November 2007.

*Researcher, Control and Simulation Division, Faculty of Aerospace Engineering, Kluyverweg 1; J.Ellerbroek@TUDelft.nl. AIAA Member.

†Researcher, Aerospace Engineering, Simulation, Motion, and Navigation, Kluyverweg 1; O.Stroosma@TUDelft.nl. AIAA Member.

‡Associate Professor, Control and Simulation Division, Faculty of Aerospace Engineering, Kluyverweg 1; M.Mulder@TUDelft.nl. AIAA Member.

§Associate Professor, Control and Simulation Division, Faculty of Aerospace Engineering, Kluyverweg 1; M.M.vanPaassen@TUDelft.nl. AIAA Member.

ψ = yaw angle
ω_0 = sweep base frequency
ω_1 = sweep maximal frequency
ω_n = natural frequency
ω_{nm} = neuromuscular natural frequency

Subscripts

c = commanded motion
ps = pilot station
s = simulator motion
sim = simulated signal

Superscript

b = aircraft body frame of reference

I. Introduction

FROM as early as the 1960s, several studies have examined the effect of motion cues on human control performance in a yaw control task [1–7]. Because of the physical location of the pilot seat in most aircraft, recent studies investigated the influence of translational, as well as yaw, motion. All studies that included translational motion agree that the largest improvement in control performance is shown when sway motion is present. However, there is less consensus concerning the effect of yaw rotational motion on performance; results vary from no significant effects [2–4], or even significant degradations in performance [4], to significant effects when no other motion is present [5,6], and significant improvements in performance [1,5]. Also, sway motion was often perceived as yaw motion by pilots [4,5], an effect which was reproduced by Groen et al. [6] in a passive aircraft decrab experiment.

Because only a few pilots participated in these studies, and because of the mixed results for the effects of yaw motion, this study focused on the effect of lateral and yaw rotational motion on pilot perception and control behavior. It consisted of two experiments. The first experiment was a repetition of Schroeder's yaw capture experiment [4]. Data from this experiment were used in comparison with results from previous studies by Schroeder and Grant et al. [4,5]. This experiment also served as a benchmark for the SIMONA Research Simulator (SRS) for helicopter tasks. To make results comparable with the previous experiments, motion shaping filters and visual delays were used to match the SRS dynamics to NASA's vertical motion simulator (VMS).

To further examine the individual effects of yaw and translational motion on pilot control behavior, a second experiment was performed. The experiment consisted of a tracking task with added disturbance, where the resulting data were used to obtain a parametrized multiloop pilot control behavioral model [8]. The model has separate perception paths for visual, translational, and rotational motion cues, which allows for a more detailed analysis of how these cues affect performance.

The following section of this paper describes the specifics of rotational and translational motion in yaw control tasks. The third section describes the method used for measuring the SRS motion dynamics, and the derivation of shaping filters used in the first experiment. Section IV then describes the method and results for the first experiment, followed by a description of the identification method used in the second experiment. Section VI describes the method and results for the combined tracking and disturbance experiment. The final section summarizes conclusions which followed from the two experiments.

II. Yaw and Sway in Helicopter Control

In most aircraft, the pilot position is not situated in the center of rotation. Because of this, rotational motion sensed by a pilot will be accompanied by linear accelerations, see Fig. 1. The relation between yaw rotational motion r, $\dot{r}$, and the specific forces resulting from yaw motion is given by Eqs. (1) and (2):

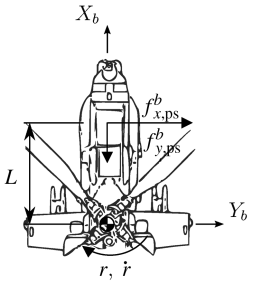

Fig. 1 Specific forces due to yaw motion at the pilot station.

$$f^b_{x,\text{ps}} = -L \cdot r^2 \tag{1}$$

$$f^b_{y,\text{ps}} = L \cdot \dot{r} \tag{2}$$

In this situation, the lateral specific force $f^b_{y,\text{ps}}$ provides the same information as the yaw rotational acceleration, and the longitudinal specific force $f^b_{x,\text{ps}}$ is related to yaw rate. The distance between the pilot and the center of rotation L determines the magnitude of these specific forces. For large distances, it can be the case that a lateral specific force cue is perceived, while rotational motion is still subthreshold. When a representative capture from Schroeder's capture task is considered [4] (see Fig. 2), it can be seen that, apart from yaw motion, lateral motion will also produce superthreshold cues [9,10]. It can therefore be considered prudent to also investigate the specific forces in this yaw control study.

The helicopter model used in Schroeder's and Grant et al.'s experiments [4,5] was a low-order representative mathematical model for an unaugmented Apache AH-64 helicopter in hover. The model behaves like a single integrator for low frequencies, and like a double integrator for frequencies above the break frequency, approximately 0.27 rad $\cdot$ s^{-1}. Thus, according to the crossover model of McRuer and Jex [11], a pilot has to generate lead when the system to be controlled behaves like a second-order system in the crossover region. For the Apache model, this means that the pilot has to perceive yaw error for low frequencies, and rate and error at frequencies above the break frequency. A human controller can obtain information on the yaw error visually, and uses both his visual rate perception and the acceleration information from his vestibular organs to obtain an estimate of velocity.

In his analysis of Schroeder's and Grant et al.'s yaw experiments [4,5], Hosman et al. provided linear models of the semicircular canal and the otolith dynamics [7] responsible for the perception of angular acceleration and specific forces, respectively:

$$H_{\text{scc}}(\omega) = \frac{1 + j\omega\tau_L}{(1 + j\omega\tau_1)(1 + j\omega\tau_2)} \tag{3}$$

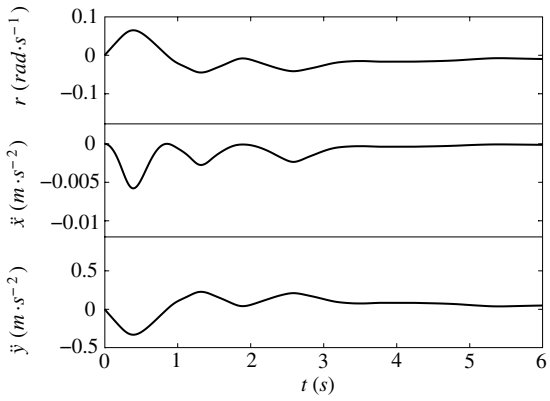

Fig. 2 Example time history for r, $\ddot{x}$, and $\ddot{y}$ from Schroeder's capture task [4], $L = 1.372$ m.

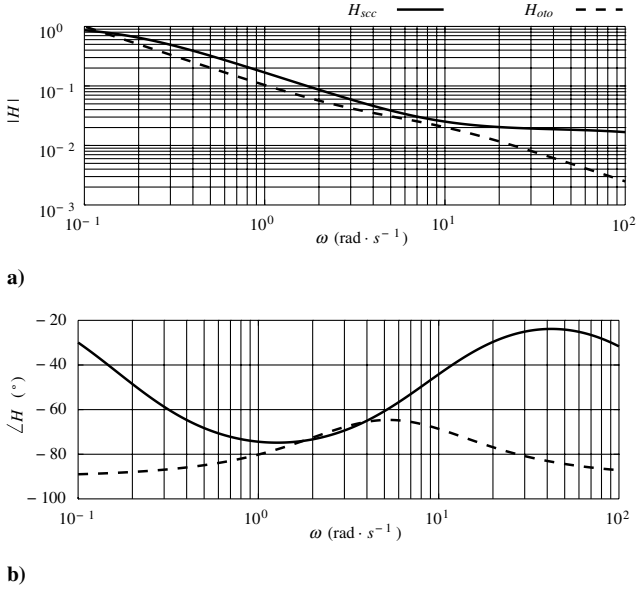

Fig. 3 Semicircular canal and otolith dynamics.

$$H_{\text{oto}}(\omega) = \frac{1}{j\omega} \cdot \frac{1 + j\omega\tau_n}{1 + j\omega\tau_3} \tag{4}$$

The semicircular canal dynamics contain a neural lead term $\tau_L = 0.11$ s, and canal lag time constants $\tau_1 = 5.9$ s and $\tau_2 = 0.005$ s. From the semicircular canal transfer function, it can be seen that output is related to angular rate, see Fig. 3. The otolith dynamics are determined by a neural lead term $\tau_n = 0.3$ s and otolith lag time constant $\tau_3 = 0.12$ s. Otolith output is related to linear acceleration, but, according to Van der Steen [12], it can be assumed that the human controller is able to integrate the otolith output to obtain an estimate of velocity. The otolith model with the integration term is shown in Fig. 3.

Because, in principle, each of the individual vestibular cues provides the required information on rotational rate, an experiment was performed to investigate the relative importance of each of these cues. To make the results comparable with previous studies from Schroeder and Grant et al. [4,5], shaping filters and added delays were used to match the characteristics of the SRS simulator with NASA's VMS. The derivation of these filters and delays is described in the next section, followed by a description of the experiment.

III. Shaping Filter and Visual Delay Selection

Results from the first experimental task were used in a comparison with the original experiment performed on NASA's VMS [4] and with Grant et al.'s repetition of this experiment [5]. Because differences in bandwidth and delay between the VMS and the SRS are significant, shaping filters were applied to the simulator commanded motion. A pure delay was inserted in the SRS visual system to match that of the VMS. The tuning of these added filters and delays are described in the following subsections.

A. Motion System

Two shaping filters were used to match rotational and translational motion, respectively. Both shaping filters consisted of two terms:

$$H_{\text{shaping}}(\omega) = H'^{-1}_{\text{SRS}}(\omega) \cdot H_{\text{app}}(\omega) \tag{5}$$

The first term, H'^{-1}_{SRS}, is the inverse of an approximation of the low-pass characteristic of the motion system dynamics of the SRS. The SRS dynamic behavior H_{SRS} can be described by a second-order low-pass filter multiplied with a pure delay:

$$H_{\text{SRS}}(\omega) = \frac{n_a(j\omega)^2 + n_b j\omega + 1}{d_a(j\omega)^2 + d_b j\omega + 1} \cdot e^{-j\omega\tau_d} \tag{6}$$

In the design of the shaping filters, only the inverse of the low-pass filter is used. The remaining delay was compensated for in the second term of the shaping filter.

The second term, H_{app}, was used to approximate the VMS dynamics, while compensating for the SRS motion system delay:

$$H_{\text{app}}(\omega) = \frac{n_a(j\omega)^2 + n_b j\omega + 1}{d_a(j\omega)^2 + d_b j\omega + 1} \tag{7}$$

Both transfer functions have been derived using measured responses from the SRS motion system to predefined frequency sweeps of the following form:

$$F(t) = A_1 \cdot \cos\left[\left(\omega_0 + \frac{\omega_1 - \omega_0}{2t_{\text{end}}}t\right)t + \phi\right] + A_2 \cdot \cos\left[\left(\frac{\omega_0}{4} + \frac{\omega_1 - (\omega_0/4)}{2t_{\text{end}}}t\right)t + \phi\right] \tag{8}$$

The frequencies that are present in the signal which drives the motion system determine in which frequency range a measured describing function is valid. Because we are interested in measuring pilot behavior, the maximum frequency was chosen well above the maximum frequency at which a pilot can still control: $\omega_1 = 24$ rad · s^{-1}. The lower bound for the frequency sweep is determined by the excursion limits of the motion system, and was set at $\omega_0 = 0.7$ rad · s^{-1}. The amplitudes $A_1 = 0.055$ m and $A_2 = 0.007$ m were selected using a inverse-kinematic model determining the leg excursions of the SRS. The phase ϕ was chosen at $\phi = 270$ deg, so that the sweep started at zero. The frequency sweeps were performed with the Apache model in the loop.

The rotational and translational shaping filters were derived in two steps. First, the parameters for the SRS low-pass characteristic were determined for each degree of freedom (yaw, sway, and surge in this study) by minimizing the following cost function:

$$J(\underline{\theta}) = \sum_{\omega=\omega_0}^{\omega_1} (|H'_{\text{SRS}}(\omega, \underline{\theta})| - |\tilde{H}_{\text{SRS}}(\omega)|)^2 \tag{9}$$

Here, $\tilde{H}_{\text{SRS}}$ is the frequency response for the SRS motion system measured with the frequency sweep, and $\underline{\theta}$ is the parameter vector $[n_a, n_b, d_a, d_b]$. From this analysis, it followed that differences between platform surge and sway motion could be neglected. The frequency sweep was also used to measure the platform response in the combined rotational and translational motion condition. The differences in response with respect to the one-axis motion conditions were marginal, and shaping filters were kept constant across motion conditions.

A comparison of simulated model data and actual sweep measurement data can be used to assess the quality of the linear models. Table 1 shows the percentage of model remnant power as a measure of model quality, averaged over multiple measurements. These percentages were calculated using the mean squared error between platform motion simulated by the linear model and measured actual platform motion:

$$n_\psi = \frac{\text{rms}(\dot{r}_l - \dot{r}_m)}{\text{rms}(\dot{r}_l)} \cdot 100\% \tag{10}$$

$$n_y = \frac{\text{rms}(\ddot{y}_l - \ddot{y}_m)}{\text{rms}(\ddot{y}_l)} \cdot 100\% \tag{11}$$

Table 1 SRS model remnant

Condition	ψ		y	
	$\bar{n}$, %	σ_n, %	$\bar{n}$, %	σ_n, %
Yaw only	8.79	0.49	——	——
Sway only	——	——	6.23	0.32
Full motion	8.82	0.43	14.42	0.97

Here, $\dot{r}_l$ and $\ddot{y}_l$ are the yaw and sway motion simulated with the linear model, and $\dot{r}_m$ and $\ddot{y}_m$ are the actual yaw and sway motion measured from the motion platform.

It can be seen that the linear model for sway motion describes platform motion less accurately when rotational motion is added. This can be at least partly explained by the fact that, for synergistic motion platforms, the different degrees of freedom are not uncoupled. Adding yaw rotational motion will have an effect on the sway motion presented by the platform [13].

Second, transfer function H_{app} was determined for rotational and translational shaping functions by minimizing the following cost function:

$$J(\underline{\theta}) = \sum_{\omega=\omega_0}^{\omega_1} |H'^{-1}_{\text{SRS}}(\omega) \cdot H_{\text{app}}(\omega, \underline{\theta}) \cdot \tilde{H}_{\text{SRS}}(\omega) - H_{\text{VMS}}(\omega)|^2 \quad (12)$$

Again, $\tilde{H}_{\text{SRS}}$ is the frequency response for the SRS motion system measured with the frequency sweep, and $\underline{\theta}$ is the parameter vector $[n_a, n_b, d_a, d_b]$. H_{VMS} is a low-order approximation of the lateral and yaw dynamics of the NASA VMS motion system, which has been derived by Schroeder [4]:

$$H_{\text{VMS}}(\omega) = \frac{1}{(1/11^2)(j\omega)^2 + (2 \cdot 0.6/11) \cdot j\omega + 1} \quad (13)$$

The initial values for $\underline{\theta}$ were chosen to match the values of H_{VMS}. A second frequency sweep was used to verify the derived shaping filters. The resulting filter parameters are summarized in Table 2.

B. Visual System

Dynamics for visual systems can generally be regarded as a pure delay. This delay arises due to transport delays, image calculation time, and the time it takes to perform hardware geometry transformation. For the VMS, Schroeder measured a visual delay of 86 ms [4]. The lumped time delay of the SRS visual system was measured using a new visual delay measurement system (VDMS) [14]. This system relies on manual visual sampling of a sinusoidal signal, and comparing its phase to a reference signal, provided by high-rate shutter glasses.

A phase difference between the refresh of the shutter glasses and the attitude signal displayed by the visual system will yield an alternating image as viewed by the VDMS operator. The delay of the visual system can then be found by varying the pulse delay of the shutter glasses until the perceived image appears stationary.

Using this system, the SRS visual delay was measured at three frequencies: 2, 4, and 8 Hz. Using three different subjects, this yielded an average delay τ_v of approximately 25–30 ms. Hence, an additional delay needed to be added to the SRS visual system to mimic the VMS visual system dynamics. To this purpose, each visual node read the network-broadcasted position data six time frames into the past. With a calculation update rate of 100 Hz, this resulted in an added visual delay of 60 ms, making the total visual system delay 85–90 ms. The added delay was verified using the same measurement technique.

IV. Experiment 1: Yaw Capture Task

To further investigate the mixed results found for the influence of yaw rotational and translational motion in yaw control tasks, Schroeder's original yaw capture task [4] was repeated. This task can also be considered a benchmark of the SRS simulator. Results were compared with the Schroeder and Grant et al. yaw capture studies [4,5]; similar findings would increase confidence in the SRS as a research simulator and reliability of all three studies.

Table 2 SRS dynamics and shaping filter parameters

		n_a	n_b	d_a	d_b
Rotational	$H_{\text{shap},\psi}$	0.0020	0.0471	0.0077	0.0982
	$H_{\text{SRS},\psi}$	1.8197	20.345	1.3862	20.619
Translational	$H_{\text{shap},t}$	0.0012	0.0374	0.0075	0.1019
	$H_{\text{SRS},t}$	0.0102	0.0596	0.0102	0.0533

A. Method

To evaluate the influence of yaw rotational and translational motion, a yaw capture task was performed with five different conditions of motion. The first four conditions were based on the conditions from Schroeder's experiment [4] (see Fig. 4): no motion, yaw rotational motion only, translational motion only, and full motion. In these conditions, motion shaping filters and an added visual system delay were used to match the responses of NASA's VMS in the original experiment. By creating similar conditions, the results can be used to validate the SRS simulator in a comparison with the VMS.

In addition to these four conditions, the experiment also featured a "one-to-one" motion condition. This condition did not have any shaping or washout filters, nor any added delays. This was possible because the motion pattern fits within the available motion space of the SRS. Because captures are always done from either the left or right toward the center, an overshoot by the pilot is not likely to encounter the limits of the motion system. This condition should show whether the higher bandwidth and lower delays of the SRS simulator have any influence on pilot performance, workload, and motion fidelity, in the capture task.

1. *Apparatus: SIMONA Research Simulator*

The experiment was performed on the SIMONA Research Simulator of Delft University of Technology. The SRS is a 6 degrees-of-freedom research flight simulator, with a hydraulic hexapod motion system. Its dynamic behavior can be described by a second-order low-pass filter multiplied with a pure delay of 30 ms in the translational axes, and 40 ms for yaw motion. The low-pass filter parameters are shown in Table 2.

Shaping filters were used to match the SRS motion to the motion dynamics of NASA's VMS simulator (see Sec. III.A). The parameters for the shaping filters are summarized in Table 2. In addition to the shaping filters, classical, second-order washout filters were applied, with parameters identical to the filters used in Schroeder's experiment [4], see Table 3.

The SRS visual system consists of three channels, each driving one liquid crystal display (LCD) projector, rendering images at a resolution of 1280×1024 pixels. Image generation of the nodes is synchronized using a hardware frame-locking system. Table 4 shows a summary of the visual hardware specifications for the SRS, VMS, and University of Toronto Institute for Aerospace Studies (UTIAS) simulators. As described in Sec. III.B, the SRS visual system delay was increased to match the ± 86 ms visual delay of NASA's VMS.

Figure 5 shows a comparison of the field of view for the UTIAS, VMS, and SRS visual systems. When compared with the VMS visual, the SRS field of view is wider, but does not extend as low as the VMS does. Although it can be argued that a downward view provides important cues in helicopter flight, the tasks in this experiment were presented at eye level, with little to no additional cues in the bottom part of the outside visual.

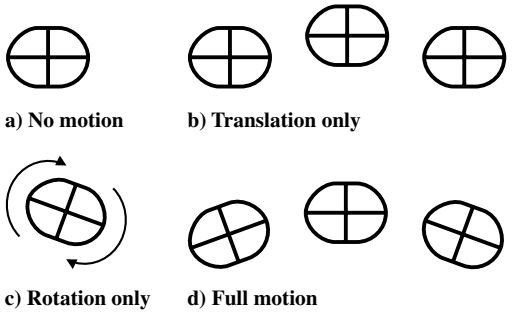

Fig. 4 Experimental motion conditions.

Table 3 SRS washout filter parameters

		No motion	Translational	Yaw	Full motion
Yaw	K, –	0	0	1.0	1.0
	ω_n, rad · s^{-1}	——	——	10^{-5}	10^{-5}
	ζ, –	——	——	0.7	0.7
Surge	K, –	0	1.0	0	1.0
	ω_n, rad · s^{-1}	——	0.2	——	10^{-5}
	ζ, –	——	0.7	——	0.7
Sway	K, –	0	1.0	0	1.0
	ω_n, rad · s^{-1}	——	10^{-5}	——	10^{-5}
	ζ, –	——	0.7	——	0.7

Like the motion system and the visual, the parameters for the rudder pedals were also selected to match the dynamics of the pedals present in the VMS. A manned frequency sweep was used to measure the force-position relationship for the pedals. Because of instability in the pedals for high bandwidth, the NASA parameters could not be directly applied to the SRS pedal system. Through a process of trial-and-error, a reduced bandwidth of $\omega_n = 13.43$ rad · s^{-1} and a damping factor of $\zeta = 0.65$ were selected. Table 5 gives a summary of the pedal settings for the VMS, UTIAS, and SRS.

2. Vehicle Model

The vehicle model used in this experiment is the same as described by Schroeder [4]: a low-order representative mathematical model for an unaugmented Apache AH-64 helicopter in hover. With parameters converted to SI units, the model can be described by the following relation between the yaw angle in the aircraft body frame of reference ψ^b and helicopter pedal input δ_p:

$$\frac{\psi^b(\omega)}{\delta_p(\omega)} = \frac{19.45}{j\omega(j\omega + 0.27)} \tag{14}$$

Here, the angle ψ^b is in radians, and the pedal deflection δ_p is in meters. The pilot seat is located in front of the center of rotation, at an offset of $L = 1.372$ m. This introduces specific forces in the lateral and longitudinal directions, see Eqs. (1) and (2).

3. Independent Variables

Throughout the experiment, three independent variables were varied. The four motion conditions in Fig. 4 show the possible combinations of rotational and translational motion. Hence, rotational and translational motion are two factors, both with two levels: they could be either present or absent. A third factor considered motion filtering at two levels: present or absent. This factor was varied between the fourth and fifth motion conditions.

4. Experiment Design and Procedure

The experimental design can be considered as two separate parts. The first part was a repetition of Schroeder's and Grant et al.'s earlier experiments [4,5]. This was a two-factor, within-subjects, repeated-measures analysis, in which factors yaw and sway platform motion were varied, with motion filtering present. The second part was a within-subjects, repeated-measures analysis with motion filtering as a factor. This latter test was done to analyze the effect of increased motion system bandwidth, and reduced motion and visual system delays of the SRS simulator. The effect of motion filtering was evaluated only with both yaw and sway motion present. This resulted in five conditions ($2 \times 2 + 1$). During the experiment, the conditions were presented in a randomized block design. On average, the pilots required approximately 20 min to train. After training, all pilots performed each condition six times, leading to 30 trials per subject. Each trial consisted of six captures. At the end of each trial, the pilot was asked to rate workload and motion fidelity. They were also asked to report whether they sensed any translational or rotational motion, or both.

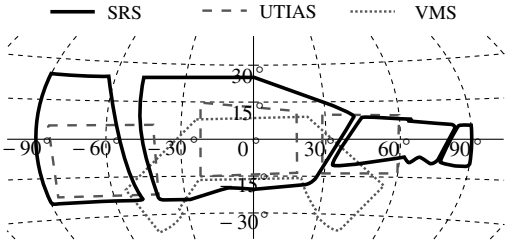

Fig. 5 Hammer–Aitoff projection of the outside visual field of view.

Effects were considered significant at a probability level $p \leq 0.05$, where p is the probability that the null hypothesis is true. Effects for which $0.05 < p \leq 0.1$ were considered marginally significant. The measurement data from Grant et al.'s experiment were used in conjunction with the data from this experiment in a mixed-mode analysis with the simulator facility as a between-subjects factor [5]. This allowed for a statistical comparison between our study and Grant et al.'s analysis.

5. Subjects and Instructions to Subjects

Six experienced helicopter pilots participated in this study: five male and one female. Two were ex-military pilots, of which one was also a certified F16 test pilot. Two participants were trauma-helicopter pilots. The remaining two pilots fly for commercial companies. The amount of flight hours per pilot ranged from 800 to 3800 h.

Subjects were asked to perform the yaw capture task. Before the experiment, they were informed that during the experiment, several settings of the motion system would be varied. For each task, pilots were asked to rapidly acquire, and stay within ±1 deg of a reference target for at least 5 s. These captures were performed from initial offsets of 15 deg to either the left or the right. Desired performance was to perform each capture with two or less overshoots. Three vertical poles marked the initial and target positions in the outside visual. The edges of these poles indicated the ±1 deg margins allowed for target capture. A head-up display showed a crosshair which provided a point of self-reference.

Table 5 Comparison of simulator rudder pedal properties

	VMS	UTIAS	SRS
Travel, m	0.09	0.07	0.05
Breakout force, N	13.34	13.34	15.0
Force gradient, N · m^{-1}	525.4	525.4	2525
Natural frequency, rad · s^{-1}	30	11	13.43
Damping ratio, –	0.5	0.5	0.65

Table 4 Comparison of simulator visual system specifications

	UTIAS	VMS	SRS
Total field of view	145 deg H × 30 deg V	110 deg H × 50 deg V	180 deg H × 65 deg V
Pixel resolution, center	1.8 arc-min	1.8 arc-min	3.18 H × 2.78 V arc-min
Transport delay	58 ms	86 ms	25–30 ms
Refresh rate	60 Hz	60 Hz interlaced	60 Hz
System hardware	Evans & Sutherland 6500Q	Evans & Sutherland CT5A	AMD64-X2 4400 + /nVidia Quadro FX5500G

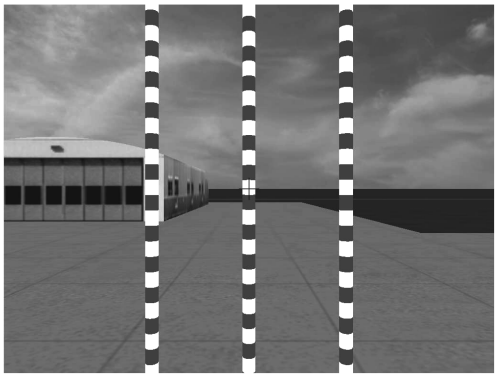

Fig. 6 Visual scene in the capture task.

The database defining the appearance of the outside visual is shown in Fig. 6. This database is the same as was used in the yaw experiment performed at UTIAS [5]. The experiment was conducted in visual meteorological conditions (VMC), and without turbulence.

6. Dependent Measures

Dependent measures for this experiment consist of the same six measures from Schroeder's and Grant et al.'s yaw capture experiments [4,5], and two additional measures.

Objective measures were the amount of overshoot, defined as a measure of performance, and the rms pedal rate defined as a measure of workload. According to Schroeder, the amount of overshoots measure is generally indicative of the level of damping, or relative stability in the pilot-vehicle system [4]. He also mentions that the pedal rate measure is often associated with workload. Overshoots were measured as the amount of traversals outside a 1 deg margin around the capture heading. Pedal rate was measured in the time period where the pilot stabilizes after capture. According to Grant et al., the first part of the capture is mainly controlled in an open-loop fashion [5]. As such, differences in motion conditions are most apparent while the pilot is stabilizing. The measurement range for each capture was therefore from the moment that the pilot first enters the ± 1 deg range, until the moment when he leaves this range to reposition for the next capture.

Subjective measures were measures of workload, motion fidelity, and the reporting of yaw and translational motion. The subjective measure of workload consisted of pilot-rated required compensation. The rating scale for compensation was derived by Schroeder from the Cooper Harper handling qualities scale [4,15]. Pilots were asked to rate motion fidelity on a three-point scale (high, medium, and low fidelity), taken from Sinacori [16].

The two additional measures considered control aggressiveness, using maximum yaw angular rate $r_{\max}$, and maximum overshoot in degrees $\psi_{\text{ov,max}}$. These measures will be described in the results section.

7. Experiment Hypotheses

Two previous yaw capture studies by Schroeder and Grant et al. [4,5] found that the largest increase in performance and motion fidelity occurred when translational motion was added. Therefore, the first hypothesis was that sway motion is the dominant cue in the control of a simulated helicopter in a yaw control task.

The second hypothesis was that the reduced delays and increased bandwidth of the SRS simulator, without shaping filters and added delays, yield better control performance and improve rated motion fidelity.

B. Results

Results for each of the measures are illustrated with figures showing the means for each of the four motion conditions and error bars representing the appropriate 95% confidence intervals. For comparison, each of the figures also includes the results from Schroeder's (NASA) and Grant et al.'s (UTIAS) experiments [4,5].

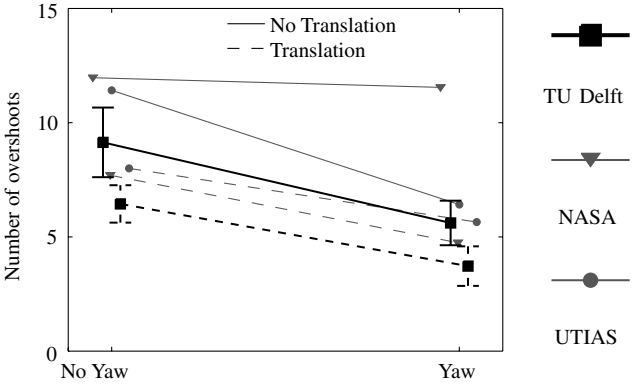

Fig. 7 Performance for yaw capture task.

Two points along the abscissa indicate the presence or absence of rotational motion. Dashed and continuous lines indicate the conditions with and without translational motion, respectively.

1. Effects of Yaw and Sway

Figure 7 shows the number of overshoots for this experiment and the NASA and UTIAS experiments. Compared to the previous studies, the number of overshoots was smaller for all of the motion conditions. However, statistical comparison with the UTIAS data did not show a significant difference between experiments for this measure. A possible reason for the lower number of overshoots could be that almost all participating pilots in this study were commercial pilots, who, compared with test pilots, tend to control more conservatively. The analysis of variance showed significant improvements for both yaw motion ($p = 0.011$) and translational motion ($p = 0.026$). Compared to Schroeder and Grant et al. [4,5], the main difference is a stronger effect of yaw; Schroeder's results showed only a marginal effect of yaw motion. Grant et al.'s analysis showed a significant effect of yaw only when sway motion was not present.

Figure 8 shows the pedal rate for the Technical University of Delft (TU Delft), NASA, and UTIAS experiments. The main difference between the current study and the results from the previous studies is the overall lower pedal rate. Again, this can be attributed to the fact that mostly commercial pilots participated in the current study; rms pedal rates for the only participating test pilot were more in line with results from the NASA and UTIAS studies. Statistical comparison with the UTIAS data did not show a significant difference between studies. This is, however, probably due to the small number of subjects in the UTIAS study. The combined analysis did reveal that the effect of sway was significantly different between simulators ($p = 0.029$), and a marginally significant difference between simulators for yaw ($p = 0.10$). In Fig. 8, this can be seen in the larger effect of yaw in the absence of sway, and the larger effect of sway in the absence of yaw for the UTIAS results as compared with the current study. For the current study, significant improvements were

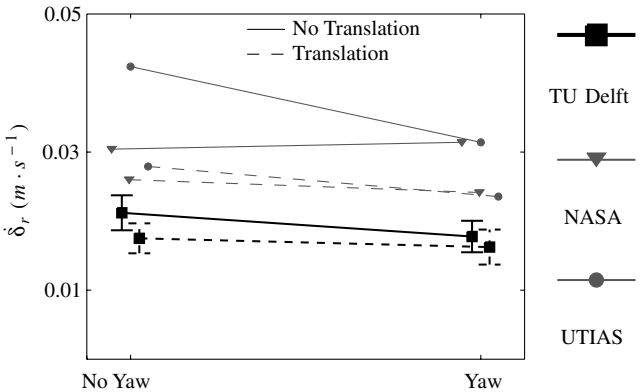

Fig. 8 Pedal rate for yaw capture task.

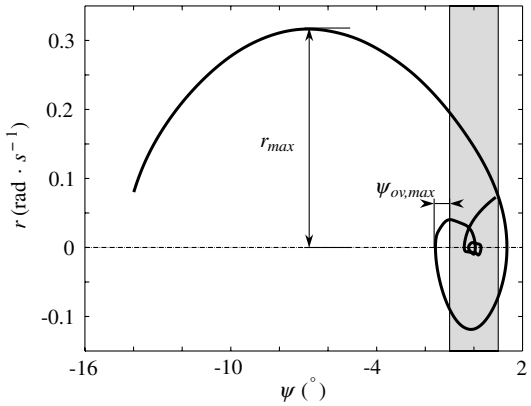

Fig. 9 Phase-plane portrait of a yaw capture.

found for both yaw ($p = 0.037$) and translational motion ($p = 0.007$). Repeated-measures analysis also showed a marginal interaction between yaw and sway ($p = 0.068$). A simple effects test revealed that the effect of yaw motion was only significant when sway motion was not present. Schroeder found that only the addition of translational motion significantly reduced pedal rate [4]. Grant et al. found a marginally significant effect of translational motion, only when yaw motion was not present [5].

Because the comparison between the UTIAS and TU Delft experiments concerns two groups of considerably different pilots, it is worthwhile to study the differences in pilot control strategies. A possible way of looking at control strategy in the capture task is with a phase-plane representation (Fig. 9), showing the trajectory that was taken for a capture, in terms of rate and position. Figure 9 also shows the maximum approach rate $r_{\max}$ and the maximum overshoot size $\psi_{\text{ov,max}}$. Although several different patterns can be observed from the data, the majority of the captures followed a pattern similar to Fig. 9. This behavior is comparable in both the UTIAS and TU Delft studies.

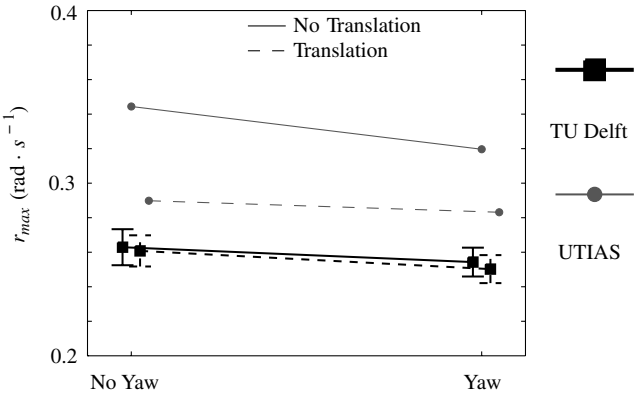

Fig. 10 Maximum yaw rate.

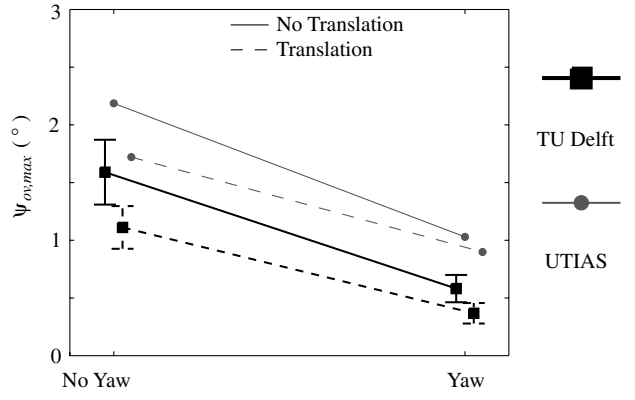

Fig. 11 Maximum overshoot.

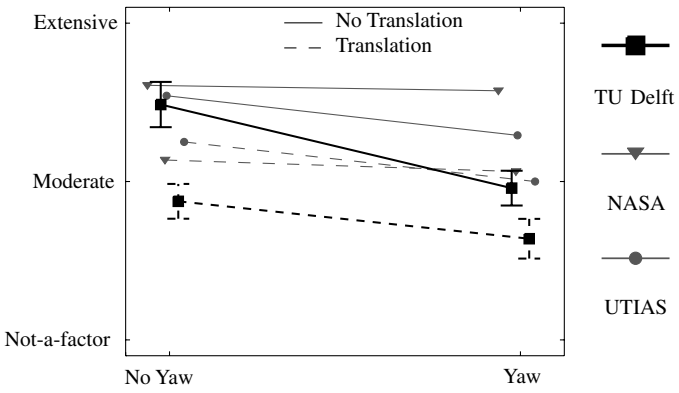

Fig. 12 Compensation for yaw capture task.

Differences between pilots can, however, be found in the degree of aggressiveness in performing the capture task. This is already clearly visible in the offset in pedal rate between the three studies, but can also be observed in maximum velocity $r_{\max}$ and in the magnitude of the overshoots $\psi_{\max}$, see Figs. 10 and 11. Repeated-measures analysis revealed a marginal effect of yaw motion on the magnitude of the overshoots ($p = 0.078$) and a significant interaction between simulator facility and sway for $r_{\max}$ ($p = 0.007$). For both measures, there was no significant main effect for the "simulator" between-subjects factor. As with pedal rate, this could be attributed to the small number of subjects in the UTIAS study.

The subjective measure of workload consisted of pilot-rated required compensation. Figure 12 shows the results for this measure. It can be seen that the current data show the same general trend as the NASA and UTIAS studies. The only noticeable difference is the overall lower workload rating. The repeated-measures analysis of the combined UTIAS and TU Delft data revealed this difference to be significant ($p = 0.016$). This overall lower workload rating can be attributed to three factors. First, because for the current study, pilots tended to control more conservatively, workload is likely to be lower. Second, there is the difference in background; pilots with different occupations will interpret the rating scale differently. The third factor is the difference in language. The pilot briefing for the current study showed the labels for the rating scale in English, with descriptions for each label in Dutch. Although these descriptions were translated from the original UTIAS briefing, the difference in language could cause a difference in interpretation. For the current study, both yaw and translational motion significantly reduced rated workload (0.015 and $p = 0.007$, respectively). Repeated-measures analysis also indicated a marginally significant interaction between yaw and sway; however, a simple effects test did not reduce the significance of either yaw or sway. In contrast, Grant et al. found a significant improvement only when translational motion was added [5]. Schroeder found no significant effects for either yaw or sway motion on pilot-rated workload [4].

Figure 13 shows the results for the motion fidelity subjective measure. The trends for yaw and translational motion compare well with NASA and UTIAS results; repeated-measures analysis of the combined UTIAS and TU Delft data did not reveal any significant between-subjects effects. For the current study, both yaw motion and translational motion increased motion fidelity significantly ($p = 0.018$ and $p = 0.034$, respectively).

The remaining two subjective measures considered pilot reporting of the presence of any translational or rotational motion during each trial. These questions resulted in several considerably different interpretations by the six pilots. Only two pilots responded in a similar fashion compared with the NASA and UTIAS studies. Their results indicate a small increase in the reporting of rotation and translation when the other type of motion was present, and a large increase when the reported type of motion was actually present. Two subjects never reported any rotation, of which, one did report translation consistently in all of the conditions. One subject never reported translation, but reported rotation in all but the no-motion condition. Another subject reported rotation similar to the UTIAS

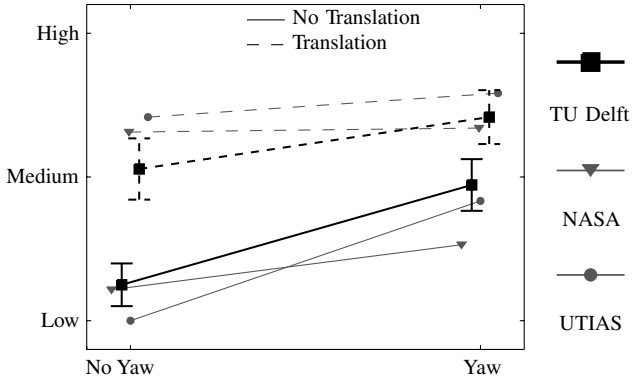

Fig. 13 Motion fidelity for yaw capture task.

and NASA studies, but reported translation only in the translation-only case. Because of this large spread, a repeated-measures analysis on the complete data would not have any significance. Apparently, without any foreknowledge of the motion conditions in an experiment, these questions appear to be easily misinterpreted. NASA and UTIAS studies reported better results for these questions, but the NASA subjects were all test pilots, and the UTIAS subjects were informed on the experimental conditions before the experiment.

2. Effects of Simulator Bandwidth and Delay

The second test regarded the effect of the presence of shaping filters and added delays. The same eight measures were used to compare two conditions. Both conditions presented full yaw and sway motion, but only one condition used shaping and washout filtering for motion, and an added delay for the visual. Although all metrics show a positive trend for the added bandwidth and reduced delay, differences are small. Repeated-measures analysis revealed only a marginally significant effect of filtering on rated motion fidelity ($p = 0.10$).

C. Discussion

Table 6 shows a summary of the results for the current yaw capture experiment, compared with earlier experiments from Schroeder [4] and Grant et al. [5]. From this table, it can be seen that, for sway motion, the results are in general agreement between studies. For yaw motion, however, the current study found larger effects for all of the considered metrics. This similarity in influence of the yaw and sway cues refutes the first hypothesis.

In his yaw experiment paper, Grant et al. mentioned that the different significant effects found in the UTIAS and NASA studies could be the result of the small sample size in both studies, and that both studies found only a subset of the effects of yaw and sway [5]. To increase the power of the current study, combined data from the current study and Grant et al.'s data were used together in a mixed statistical analysis. This comparison did not reduce any of the effects in the current study, which supports the current results found for yaw motion. It also illustrates Grant et al.'s notion that the low amount of significant effects could, at least in part, be the result of the small sample size of the NASA and UTIAS studies.

Grant et al. [5] hypothesized that a group of (test) pilots recruited for an experiment will in general not be a random sample of the entire test pilot population, and that pilots recruited in groups tend to have common controlling styles. This phenomenon was also observed between the UTIAS and TU Delft pilot groups; the combined analysis revealed overall offsets between studies for compensation ratings, pedal rate, and in the number of overshoots.

This experiment also considered the effects of higher bandwidth and lower delays of the SRS simulator. Although all metrics showed a positive trend due to the increased simulator performance, none of these effects were significant. Apparently, the largest improvement in pilot performance is gained with the addition of motion itself. These results are, however, not conclusive toward proof or refutal of the second hypothesis.

When replicating an experiment, the technical characteristics of the apparatus can be replicated relatively well, assuming those characteristics are properly documented. But human-in-the-loop experiments always have a highly variable component in the human pilot. The overall offsets found between the UTIAS and TU Delft studies indicate that the human factor warrants at least as much attention as the purely technical aspects when designing these kinds of experiments.

Because, in contrast to Schroeder's and Grant et al.'s findings [4,5], yaw and sway seem to play more equal roles in the improvement of pilot control performance, a second experiment was performed. In this experiment, the individual rotational and translational perception paths were identified in a multiloop pilot control model, as well as their influence on pilot control behavior. The identification method and pilot model are introduced in the next section, followed by a detailed description of the second experiment in Sec. VI.

V. Multiloop Pilot Model Identification

In tasks such as a disturbance-rejection, or a target-tracking task, a pilot closes the control loop, feeding back the perceived cues to stabilize the vehicle and improve task performance. Although a human pilot is essentially a nonlinear and time-variant system, control behavior can be described with a quasi-linear, time-invariant model, provided that the pilot is adequately trained.

In the analysis of the effects of motion on the control behavior of a pilot, a cybernetic, model-based approach can provide valuable insights. In his analysis of Schroeder's and Grant et al.'s yaw control experiments [4,5], Hosman et al. used the assumption that a pilot will optimize his behavior to achieve good task performance and effective control effort [7]. Based on this assumption, Hosman et al. predicted model parameters by minimizing a heuristic cost function based on task performance and control effort. However, additional insight can be gained from the identification of a pilot model from measured data. A detailed analysis can be made of the way the individual cues contribute to the pilot's control behavior [8,17].

The estimation of pilot control models in this study was done in three steps: first, the data from the measurement runs were

Table 6 Comparison of results for TU Delft, UTIAS, and NASA yaw capture experiments

	Yaw			Translation			Yaw × trans			Shaping
	TU Delft	UTIAS	NASA	TU Delft	UTIAS	NASA	TU Delft	UTIAS	NASA	
Overshoots	S	S^{-}	M	S	M^{-}	S	——	S	——	——
Pedal Rate	S^{-}	——	——	S	M^{-}	S	M	——	——	——
Compensation	S	——	——	S	S	——	M	——	——	——
Fidelity	S	M^{-}	——	S	S	S	——	S	——	M
Max Yaw Rate	——	——	——	——	——	——	——	——	——	——
Max Overshoot	M	——	——	——	——	——	——	——	——	——

[a]S: significant
[b]S^{-}: significant when other motion not present
[c]M: marginally significant
[d]M^{-}: marginally significant when other motion not present

preprocessed to remove noise and nonlinearities as much as possible. Second, using autoregressive exogenous (ARX) time-domain estimation, continuous frequency response functions were derived for the separate sensory paths [8]. Third, the parameters for the multiloop pilot describing function were estimated. These steps are described in the following subsections. The last subsection discusses the selection of appropriate forcing functions.

A. Multiloop Pilot Model

Figure 14 shows the multiloop model that was used to describe pilot control behavior, inside the experiment control loop. It consists of three parts: the simulator dynamics, the pilot dynamics, and the Apache helicopter dynamics [Eq. (14)]. The pilot model was based on Hosman et al.'s descriptive pilot model [18], but to ensure the ability to estimate all model parameters from the experimental data, Hosman et al.'s model was simplified to contain only one visual path. The vestibular sensory dynamics H_{scc} and H_{oto} are described in Eqs. (3) and (4) and were considered fixed. To model visual error and rate perception, the current study uses a lead term:

$$H_{\text{vis}}(\omega) = (1 + j\omega\tau_{L_v}) \tag{15}$$

The central nervous system is represented by the cue integration gains K_v, K_y, and K_ψ, and by the delays τ_{d_v}, τ_{d_y}, and τ_{d_ψ}. H_{nms} represents the neuromuscular dynamics:

$$H_{\text{nms}}(\omega) = \frac{\omega_{\text{nm}}^2}{(j\omega)^2 + 2\zeta_{\text{nm}}\omega_{\text{nm}}j\omega + \omega_{\text{nm}}^2} \tag{16}$$

where the natural frequency ω_{nm} is influenced by leg mass m_p and stiffness k_p, the pedal mass m_r, and the force gradient k_r settings [see Eq. (17)]. Damping ratio ζ_{nm} is influenced by leg damping B_p, mass, and stiffness, and by pedal damping B_r, mass, and force gradient settings:

$$\omega_{\text{nm}} = \sqrt{\frac{k_p + k_r}{m_p + m_r}} \tag{17}$$

$$\zeta_{\text{nm}} = \frac{B_p + B_r}{2\sqrt{(k_p + k_r)\cdot(m_p + m_r)}} \tag{18}$$

In Fig. 14, n describes the pilot remnant. According to McRuer and Jex, pilot control behavior can be described by a linear model and a remnant term n, describing the pilot's nonlinear behavior [11]. The current study only considered the pilot behavior that could be described by a linear model.

When the pilot control output δ_p is considered as the result of the perceived error $e = \psi_t - \psi^b$ and the perceived state $x = \psi^b$, two paths can be distinguished for the pilot model:

$$H_{p_e} = H_{\text{vis}} \cdot K_v \cdot e^{-j\omega\tau_d v} \cdot H_{\text{nms}} \tag{19}$$

$$H_{p_x} = [H_{\text{scc}} \cdot K_\psi \cdot e^{-j\omega\tau_d \psi} + H_{\text{oto}} \cdot K_y \cdot e^{-j\omega\tau_d y}] \cdot H_{\text{nms}} \tag{20}$$

For the four motion conditions defined by Schroeder [4] (Fig. 4), which were also used in experiment 2, the state feedback term H_{p_x} will be different. In the no-motion condition, H_{p_x} is zero, in the rotation-only condition, K_y is zero, and in the translation-only condition, K_ψ is zero.

B. Data Preprocessing

Before the identification, the measurement data were preprocessed to remove noise and nonlinearities as much as possible. The original data were sampled at 100 Hz. The first operation was averaging the data over several runs of the same condition. This operation reduces the occurrence of nonlinear outliers and bursts. Next, the first 10 s were removed from the data to allow for a stabilizing period. The resulting data was resampled, such that the Nyquist frequency was higher, but close to the bandwidth of the forcing functions. To avoid aliasing effects, the data were low-pass filtered, where the break frequency of the filter was chosen at the Nyquist frequency of the resampled data. The new sampling frequency was chosen based on the coherence between the input forcing functions, and the measured pilot control output. The coherence is a measure of how much of the inputs (here, the forcing functions ψ_t and δ_d) is linearly transmitted to the output:

$$\rho_{\psi_t\delta_p} = \frac{|S_{\psi_t\delta_p}|^2}{S_{\psi_t\psi_t} \cdot S_{\delta_p\delta_p}} \tag{21}$$

$$\rho_{\delta_d\delta_p} = \frac{|S_{\delta_d\delta_p}|^2}{S_{\delta_d\delta_d} \cdot S_{\delta_p\delta_p}} \tag{22}$$

Here, $S_{\psi_t\delta_p}$, and $S_{\delta_d\delta_p}$ are the cross-spectral densities between forcing function inputs ψ_t and δ_d, and pilot control signal δ_p. $S_{\psi_t\psi_t}$, $S_{\delta_d\delta_d}$, and $S_{\delta_p\delta_p}$ are autospectral densities of forcing function inputs ψ_t and δ_d, and pilot control signal δ_p, respectively. When the coherence at a given frequency dropped below 0.7, the data was resampled with a Nyquist frequency below that frequency.

C. Model Estimation from Measured Data

A two-step identification method was used. First, nonparametric frequency response functions of the pilot were identified from the time histories, with a multi-input single-output ARX model structure [8]. For each condition, the orders of the ARX model have been selected, based on the variance accounted for of the resulting model, and on comparison with Fourier coefficient estimates at the forcing function frequencies, determined from the same data [8]. The variance accounted for (VAF) defines the percentage of the variance of the measured δ_p that is captured by the identified linear ARX model. The VAF is given by

$$\text{VAF} = \left(1 - \frac{\sum_{k=1}^{N}(\delta_p[k] - \delta_{p,\text{sim}}[k])^2}{\sum_{k=1}^{N}\delta_p^2[k]}\right) \cdot 100\% \tag{23}$$

where $\delta_{p,\text{sim}}$ is the pilot control output simulated with the identified ARX model.

The pilot model parameters, summarized in Table 7, will be estimated from measurement data by minimizing the following cost function:

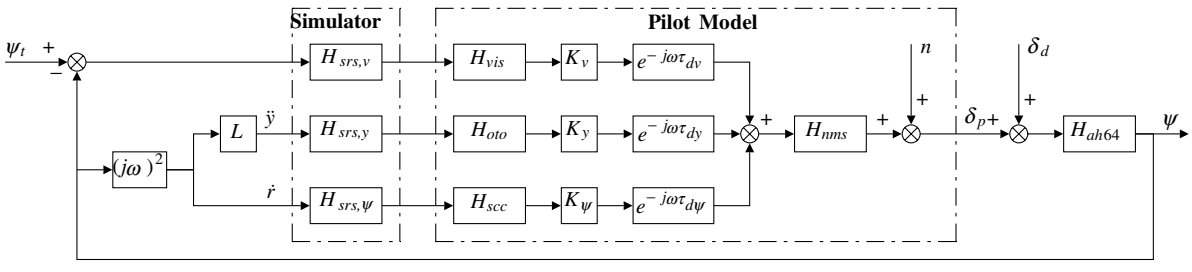

Fig. 14 Experiment closed loop.

Table 7 Pilot model estimated parameters

Parameter	Description	Unit
τ_{L_v}	visual lead time constant	s
K_v	visual perception gain	——
K_y	otolith perception gain	——
K_ψ	semicircular canal perception gain	——
τ_{d_v}	visual perception time delay	s
τ_{d_y}	otolith perception time delay	s
τ_{d_ψ}	semicircular canal perception time delay	s
ω_{nm}	neuromuscular frequency	rad · s^{-1}
ζ_{nm}	neuromuscular damping	——

$$J(\underline{\theta}) = \frac{1}{N} \cdot \sum_{\omega=\omega_0}^{N\cdot\omega_0} \frac{|\hat{H}_e[\omega] - H_e[\omega, \underline{\theta}]|^2}{\sigma_e^2[\omega]} + \frac{|\hat{H}_x[\omega] - H_x[\omega, \underline{\theta}]|^2}{\sigma_x^2[\omega]} \quad (24)$$

Here, $\hat{H}_e$ and $\hat{H}_x$ are the identified visual and vestibular paths, defined at N frequency points; σ_e and σ_x are the standard deviations for the identified $\hat{H}_e$ and $\hat{H}_x$; $\underline{\theta} = [\tau_{L_v}, K_v, K_y, K_\psi, \tau_{d_v}, \tau_{d_y}, \tau_{d_\psi}, \omega_{\text{nm}}, \zeta_{\text{nm}}]$ is the parameter vector that minimizes J. Note that H_e and H_x describe the parametric visual and vestibular paths, combined with the simulator dynamics:

$$H_e = H_{\text{srs},v} \cdot \{(1 + \tau_{L_v} j\omega) \cdot K_v \cdot e^{-j\omega\tau_{dv}} \cdot H_{\text{nms}}\} \quad (25)$$

$$H_x = (j\omega)^2 \cdot (L \cdot H_{\text{srs},y} \cdot \{H_{\text{oto}} \cdot K_y \cdot e^{-j\omega\tau_{dy}} \cdot H_{\text{nms}}\} + H_{\text{srs},\psi} \cdot \{H_{\text{scc}} \cdot K_\psi \cdot e^{-j\omega\tau_{d\psi}} \cdot H_{\text{nms}}\}) \quad (26)$$

Again, in the yaw-only and the sway-only motion conditions, $H_{\text{srs},y}$ and $H_{\text{srs},\psi}$ were set to zero, respectively. In these conditions, parameters describing the corresponding vestibular path were omitted from the estimation process.

D. Forcing Function Selection

One of the most crucial parts in an experiment in which a linear model is derived from human control behavior is the type of forcing function. Forcing functions defining tracking and disturbance signals (ψ_t and δ_d in Fig. 14, respectively) should not induce excessive nonlinear or regressed behavior in a pilot, but still should provide enough bandwidth to be able to fit a reliable model to the measured data. This experiment used sum-of-sines type forcing functions. This is the most commonly used type of forcing function, and is tuned based on bandwidth and power [11].

The tracking and disturbance forcing functions were designed as follows [19]: First, a measurement interval was selected. For practical reasons, anything under 2 min is desirable. For the Fourier coefficient method, it was desirable to round the number of samples in the measurement interval to the nearest power of two. For $T_{\text{desired}} = 120$ s, this leads to a measurement interval of $T_{\text{meas}} = 81.92$ s. With several additional seconds lead-in and lead-out time, an experimental time interval of $T_{\text{tot}} = 100$ s was selected. From the measurement interval, the base frequency can be derived:

$$f_b = \frac{1}{2\pi T_{\text{meas}}} \quad (27)$$

Next, 13 approximately evenly spaced frequencies were chosen as initial tracking signal frequencies. With these frequencies in mind, 13 prime multiples of the base frequency could be selected close to the 13 chosen frequencies, while keeping at least one prime index in between each selected frequency. The 13 frequencies for the disturbance were then chosen at prime indices centered between the tracking frequencies.

The magnitude distribution for the tracking function is chosen similar to a McRuer spectrum [11]. According to McRuer and Jex's *Verbal Adjustment Rules* [11], the dynamics of the controlled element and the forcing function bandwidth influence the occurrence of crossover regression. If forcing function bandwidth is chosen too high, a human controller will revert to regressive control behavior. Using the verbal adjustment rules, a cutoff frequency of $\omega_i = 2$ rad · s^{-1} was chosen. Amplitudes of sines with $\omega_i > 2$ rad · s^{-1} were chosen an order of magnitude lower than the sines with $\omega_i < 2$ rad · s^{-1}. Because the disturbance signal passes through the system dynamics before being sensed by the pilot, its magnitude distribution can be chosen as a flat spectrum.

Finally, the phases for the sines in the tracking and disturbance signals are chosen. To find a distribution that induces nonlinear control behavior as little as possible, phases are selected based on maximum values of the forcing function signal and its first two derivatives. First, 10,000 sets of randomly generated phases are used to calculate respective sets of maxima. Then, a subset of results is selected from phase sets which have their maximum values in a 0.005% region around the most common value for the signal itself, as well as its derivatives. From this set, the set of phases is selected which results in a forcing function that best matches a normal distribution. The resulting tracking and disturbance functions are summarized in Table 8.

Table 8 Forcing function parameters

ID	Frequency, rad · s^{-1}	Amplitude, m	Phase, rad
Disturbance			
0	0.53689	0.001	3.5803
1	0.99709	0.001	1.1036
2	1.45728	0.001	4.3267
3	2.22427	0.001	2.7792
4	2.83786	0.001	3.8042
5	3.29806	0.001	3.7394
6	4.06505	0.001	1.1676
7	5.13884	0.001	4.9589
8	6.82621	0.001	4.6632
9	8.66699	0.001	1.8763
10	12.0417	0.001	2.0372
11	16.1835	0.001	3.2665
12	20.7854	0.001	2.1173
Tracking			
ID	Frequency, rad · s^{-1}	Amplitude, rad	Phase, rad
0	0.38350	0.02857	5.9865
1	0.84369	0.02857	4.4238
2	1.30388	0.02857	5.9934
3	1.76408	0.02857	3.7583
4	2.37767	0.00286	5.2825
5	3.14466	0.00286	2.7823
6	3.60485	0.00286	5.2579
7	4.52524	0.00286	3.2591
8	5.59903	0.00143	1.3955
9	7.90000	0.00143	2.3618
10	10.5078	0.00143	5.6460
11	13.7291	0.00143	2.6955
12	18.3311	0.00143	1.2539

VI. Experiment 2: Combined Tracking and Disturbance Task

A second experiment was performed to investigate the separate effects of visual and motion feedback on pilot performance. A combined target-tracking and disturbance-rejection task was used to model the effects of yaw and sway in a multimodal pilot control behavior model. This was a new experiment, and could therefore not be completely compared with Schroeder's and Grant et al.'s studies [4,5].

A. Method

The combined target-tracking and disturbance-rejection task used motion conditions based on the motion conditions from Schroeder's experiment [4] (see Fig. 4): no motion, yaw rotational motion only, translational motion only, and full motion. The results from this task were used in the identification of multiloop describing functions of pilot control behavior. No shaping or washout filters were applied in any of these four motion conditions, and no extra delays were added

to the visual system. A consequence of not using any washout filters adds a complication for the translation-only motion condition. For yaw turns about a point, the longitudinal acceleration at the pilots station is always negative. Because of this, the simulator cab would quickly exceed its available longitudinal displacement. The translation-only motion condition therefore included only the lateral translation component.

1. Apparatus

This experiment was performed on the SIMONA Research Simulator. No washout filters, shaping filters, or added delays were used; one-to-one motion was presented in all experimental conditions.

The SRS dynamic behavior can be described by a second-order low-pass filter multiplied with a pure delay of 30 ms in the translational axes, and 40 ms for yaw motion. The parameters for the low-pass characteristics can be found in Table 2. The delay of the visual system was measured to be approximately 30 ms. Section III.B described the measurement method for this delay. Rudder pedal properties were set equal to those in the yaw capture experiment (see Table 5).

2. Vehicle Model

The vehicle model used in this experiment is equal to the one used in the yaw capture experiment: a low-order representative mathematical model for an unaugmented AH-64 helicopter in hover, see Eq. (14). The offset between pilot seat and center of rotation was kept at $L = 1.372$ m.

3. Independent Variables

Throughout the experiment, two independent variables were varied. Rotational and translational platform motion had two levels: they could be either present or absent.

4. Experiment Design and Procedure

The experimental design was a two-factor, within-subjects repeated measures, in which factors yaw and sway platform motion were varied. This resulted in the four conditions (2×2) shown in Fig. 4. During the experiment, the conditions were presented in a randomized block design. Pilots were required to train each condition eight times to reach a stable level of performance. After training, all pilots performed each condition another eight times, leading to 32 trials per subject. Measurements for this task did not include any subjective ratings.

Effects were considered significant for $p \leq 0.05$, where p is the probability that the null hypothesis is true. Effects for which $0.05 < p \leq 0.1$ were considered marginally significant.

5. Subjects and Instructions to Subjects

The same six pilots participated in the second experiment. During each task, pilots were asked to track a leading helicopter for 100 s per trial. The lead helicopter yawed randomly about the center of mass of the pilot's own helicopter, at a distance of 45 m. In addition, simulated turbulence was added to the pilot's input. By introducing these two input signals, ψ_t and δ_d, respectively, a multiloop pilot model can be identified [8,17]. The pilots reference of position was given by a crosshair on the centerline of the helicopter. A circular target attached to the rear of the lead helicopter (Fig. 15) indicated the range of desired performance of ± 1.3 deg. Satisfactory performance was to keep the crosshair within ± 2.6 deg of the target. For this task, the same visual database was used as for the yaw capture task.

6. Dependent Measures

The combined target-tracking and disturbance-rejection task was analyzed using measures of performance and workload, and through evaluation of the effects of the different types of motion on the characteristic parameters of the identified pilot control model. The rms tracking error $\psi_t - \psi^b$ was used as a measure of performance for the dual task. The rms pedal rate was used as a measure of workload. The model parameters describe human visual and neuromuscular dynamics and central nervous system perception gains and delays for the visual, otolith, and semicircular canal paths. The parameters have been introduced in Sec. V.C. Data from the fourth motion condition was used to compare the percentage of time that occurring yaw and sway motion was at superthreshold. Heerspink et al. measured the following thresholds: 0.0166 rad $\cdot$ s^{-1} for yaw and 0.0743 m $\cdot$ s^{-2} for sway motion [10].

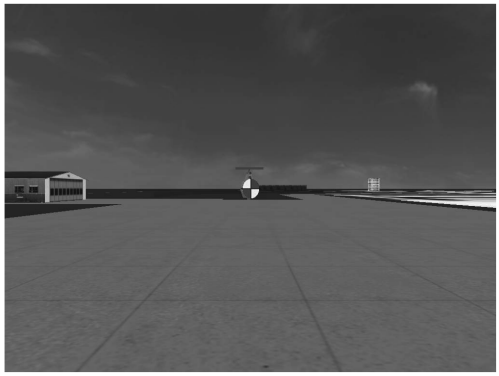

Fig. 15 Visual scene in the dual task.

7. Experiment Hypothesis

The yaw capture experiment found similar effects of translational and rotational motion on pilot performance. Also, Grant et al.'s results for a yaw disturbance task and a yaw tracking task show effects of both translational and rotational motion on pilot performance [5]. It was therefore hypothesized that translational motion and rotational motion cues have comparable effects on a pilots control behavior.

B. Results

The rms tracking error was used as a measure of performance for the dual task, shown in Fig. 16. Repeated-measures analysis revealed significant effects for yaw ($p = 0.04$) and sway ($p = 0.00$), but also a significant interaction between yaw and sway ($p = 0.05$). A simple effects test indicated that yaw motion significantly improved performance only when sway motion was not present. Although Grant et al. did not perform a combined task, the dual task and Grant et al.'s tracking task should be comparable [5]; in the current experiment, the disturbance signal was small compared to the tracking signal. In Grant et al.'s tracking task, the performance measure showed a similar trend: sway motion improved performance significantly when yaw was present, and yaw motion improved performance marginally when sway motion was present.

As with the yaw capture task, rms pedal rate was used as a measure of workload, shown in Fig. 17. Repeated-measures analysis indicated that only sway marginally reduced rms pedal rate. This trend is

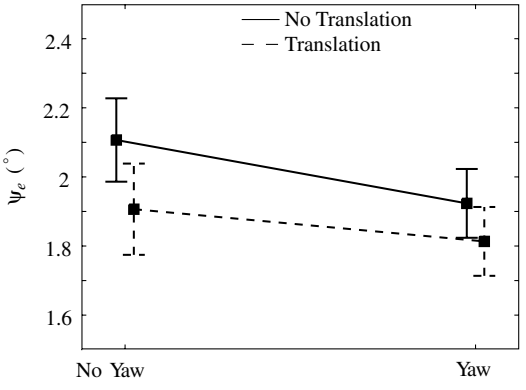

Fig. 16 Performance for dual task.

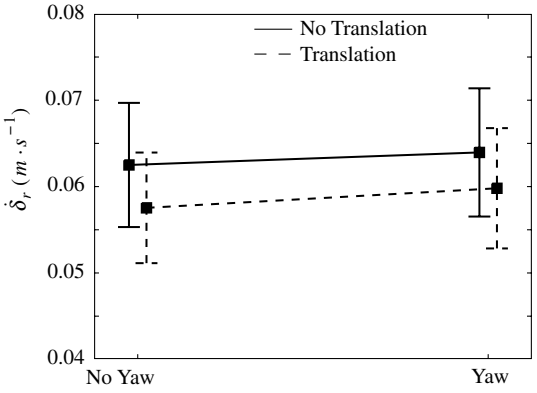

Fig. 17 Pedal rate for dual task.

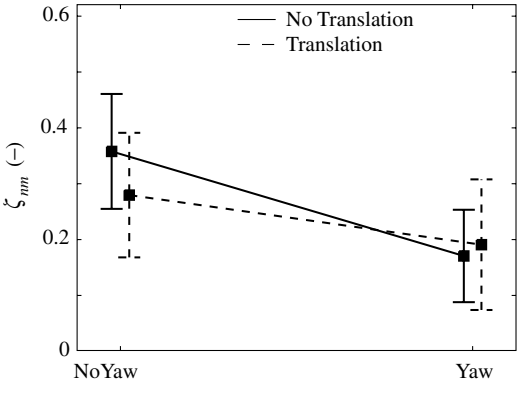

Fig. 19 Neuromuscular damping.

also comparable with Grant et al.'s tracking task. Grant et al. found no significant effects of motion on pedal rate for the tracking task.

The analysis of the effects of motion based on the estimated parameters of the pilot control model can be split into three parts: the visual parameters, the vestibular parameters, and the neuromuscular parameters. The vestibular otolith and semicircular canal paths were only present in the estimated model when their respective motion type (sway and yaw, respectively) was present. Furthermore, because there were only two deterministic signals driving the closed loop (the tracking and disturbance signals), and because otolith and canal dynamics are similar in the frequency range where the pilot model is estimated, otolith and canal path parameters could not be estimated together reliably in the analysis of the full motion condition. Because of this, comparison of the effects of the two types of motion should really only be done with parameters which are present in the pilot model for all of the motion conditions.

Figure 18 shows the parametrized H_{p_e} and H_{p_x} for one of the pilots. The figure clearly shows the visual lead that is generated in the no-motion condition, as well as the increase in neuromuscular damping and the reduction in neuromuscular bandwidth in this condition. It can also be seen that with full motion, the pilot was able to increase his visual gain to decrease the tracking error.

Figures 19 and 20 show the estimated parameters for neuromuscular damping and natural frequency, respectively. These parameters are influenced by the mass, spring, and damping properties of the legs, but also by the settings of the rudder pedals, see Eqs. (17) and (18). A pilot can influence effective leg stiffness by co-contraction of antagonistic muscles. He can also influence leg damping by preloading the rudder pedals with both feet.

From Fig. 20, it can be seen that the neuromuscular natural frequency is relatively constant at $\omega_{\text{nm}} = 9$ rad $\cdot$ s^{-1}. This result is to be expected; a pilot can only change ω_{nm} by changing his stiffness. This change would have to be large to have a significant effect on ω_{nm}. Repeated-measures analysis did reveal a significant increase for ω_{nm} when yaw motion was added, but only when sway motion was not present ($p = 0.04$). The neuromuscular damping varies more between conditions, with a significant reduction when yaw motion was present ($p = 0.002$), and a marginal effect of sway, but only when yaw motion was not present ($p = 0.08$). The reduction in damping corresponds with the increase in natural frequency; an

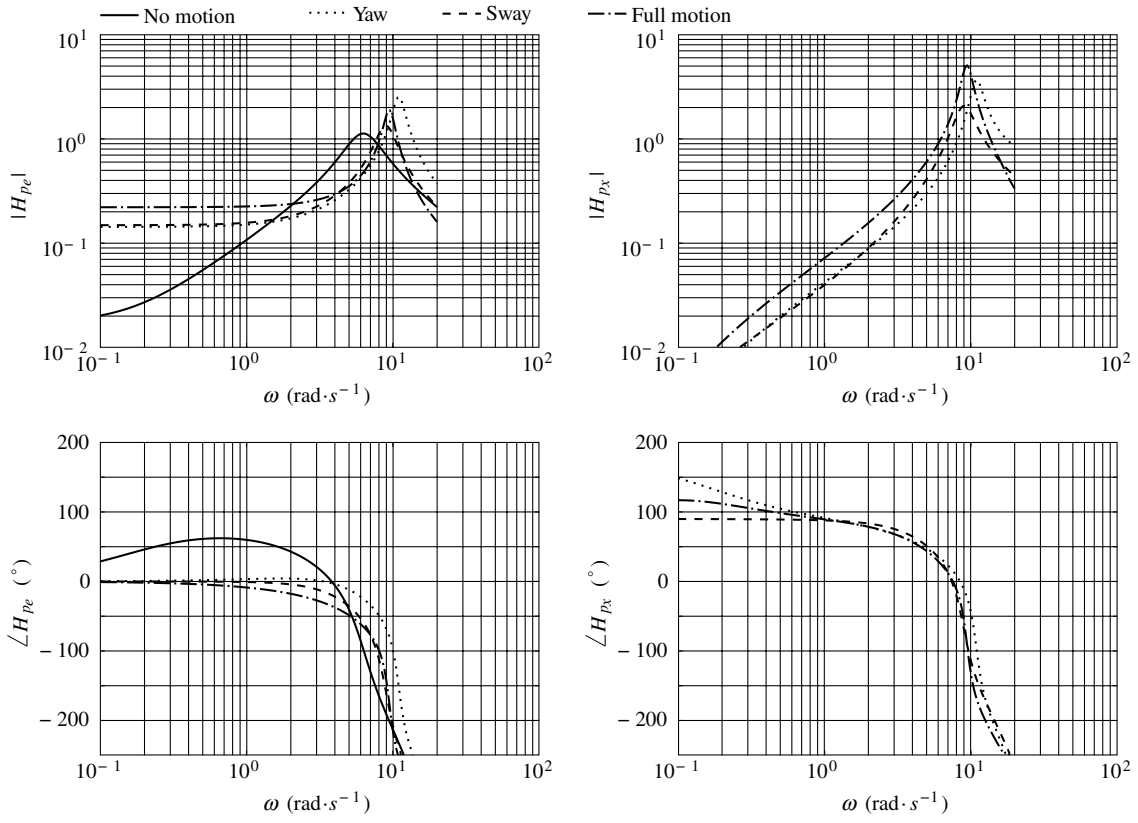

Fig. 18 H_{p_e} and H_{p_x} in the no-motion, yaw, and sway conditions for one pilot.

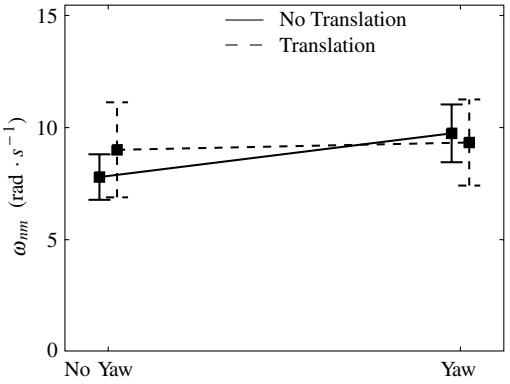

Fig. 20 Neuromuscular natural frequency.

increase in effective leg stiffness increases natural frequency, but, with constant damping B, reduces the damping factor ζ_{nm}. An increase in ω_{nm} and a decrease in ζ_{nm} together, are generally indicative of a control strategy in which a pilot is working on a reduction of his effective time delay by increasing his neuromuscular bandwidth. It can be argued that when motion is added, the pilot is more confident in his control actions and therefore adapts this strategy to improve performance.

Figures 21 and 22 show the visual gain and lead for the four motion conditions. The first observation that can be made is the high value for τ_{L_v} in the no-motion condition; in the absence of motion, a pilot needs to generate lead visually to reach desired performance. Repeated measures indicated a significant effect of yaw on τ_{L_v} ($p = 0.004$) and a significant effect of sway when yaw motion was not present ($p = 0.01$).

From Fig. 21, it can be seen that with the addition of motion, a pilot can increase his visual gain to reduce the tracking error. Repeated measures indicated a significant increase in K_{vis} when yaw motion was added ($p = 0.002$). The effect of added sway motion was significant when yaw motion was not present ($p = 0.002$), and marginally significant when yaw motion was already present ($p = 0.07$).

Figure 23 shows the effects of motion on the product $K_{\text{vis}} \cdot \tau_{L_v}$ and the semicircular canal gain K_{scc}. The difference between these two parameters is indicative of the relative utilization of visual and vestibular cues in the estimation of rotational velocity. It can clearly be seen that with the addition of motion, vestibular cues dominate the pilot's estimation of velocity.

The effect of motion on visual delay τ_{d_V} is shown in Fig. 24. There are no significant effects of motion on the visual delay.

A possible difference in the presence of yaw and sway motion that could have an effect on performance is the amount of time in each trial that the simulated motion produces superthreshold cues. For this, the difference between rotational and translational motion depends on the distance of the pilot to the helicopter center of rotation L. Analysis of the measured data revealed that, respectively, 42% and 40% of the total time per run produced superthreshold motion for yaw and sway. This difference is, however, too small to explain any differences in influence between the two motion cues.

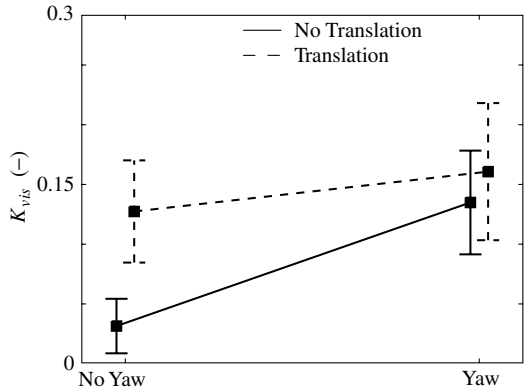

Fig. 21 Visual perception gain.

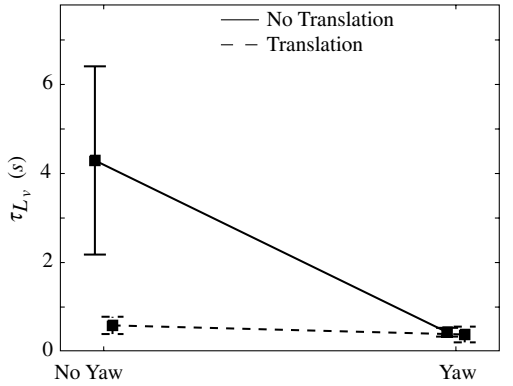

Fig. 22 Visual lead.

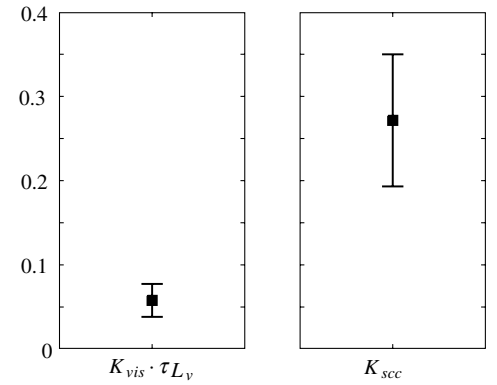

Fig. 23 Parameters $K_{\text{vis}} \cdot \tau_{L_v}$ and K_{scc} in motion condition 2.

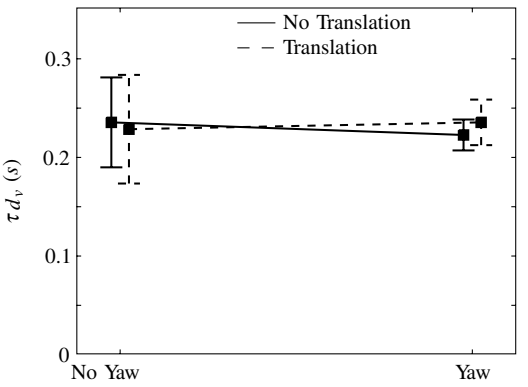

Fig. 24 Visual delay.

C. Discussion

The results for the combined tracking and disturbance experiment are summarized in Table 9. The rms tracking error and rms pedal rate were considered as measures of performance and workload, respectively. These results compare well to Grant et al.'s tracking experiment [5]: significant effects of both yaw and sway on performance, and only little effect of sway motion on the rms pedal rate.

From the resulting estimated multiloop pilot models it can be concluded that the effects of yaw and sway motion are comparable. Without motion feedback, it can be seen that a pilot uses his visual velocity estimation to generate lead: a strategy which disappears as

Table 9 Results for the combined tracking and disturbance experiment, and Grant et al.'s tracking experiment [5]

	Yaw		Sway		Yaw × sway	
	Delft	UTIAS	Delft	UTIAS	Delft	UTIAS
Tracking error	S^-	M^+	S	S^+	S	S
Pedal rate	——	——	M	——	——	——
K_{vis}	S	——	S^-	——	S	——
τ_{L_v}	S	——	S^-	——	S	——
τ_{d_v}	——	——	——	——	——	——
ζ_{nm}	S	——	M^-	——	S	——
ω_{nm}	S^-	——	——	——	M	——

[a]S: significant
[b]S^-: significant when other motion not present
[c]S^+: significant when other motion present
[d]M: marginally significant
[e]M^-: marginally significant when other motion not present
[f]M^+: marginally significant when other motion present

soon as any type of motion is added. Increased damping and reduced bandwidth is observed for the neuromuscular system in the no-motion condition. This effect is reversed with the addition of motion, although this difference was only significant for yaw motion. Also, with the addition of motion, a pilot can rely on his vestibular information in the estimation of velocity. As a result, he can increase his visual gain to reduce the tracking error. This proves the hypothesis of the second experiment.

It can be seen that, across the different motion conditions, the visual delay remains constant. This corresponds well with Hosman et al.'s assumptions in his analysis of Schroeder's and Grant et al.'s yaw experiments [7]. He assumes that this delay is the result of fixed delays such as the transport delay in the optical pathways, and a perception and decision delay in the central nervous system. Hosman et al. did, however, differentiate between visual attitude and rate perception delays, and between central visual and peripheral rate perception. These differences were not considered in the current study.

The current study also considered the relative occurrence of yaw and sway motion during a run. With the pilot seat offset by $L = 1.372$ m from the center of rotation, this resulted in 42% of the time superthreshold yaw motion, and 40% for sway motion. This difference is not large enough, however, to explain any different effects of yaw and sway. Recommendations for a follow-up study would be to obtain indifference thresholds for yaw and sway motion [20], and to use these in an analysis of yaw and sway motion in an active control task, for instance, by varying the distance of the pilot to the center of rotation.

Also, an investigation into the effects of nonlinear behavior of motion systems on experimental results is warranted. Although motion systems can be matched relatively well with shaping filters, differences that are not captured with a linear model, such as actuator noise and parasitic accelerations, can be significant and can influence experimental results.

VII. Conclusions

In the yaw capture task, translational and rotational motion had a similar effect on performance, workload, and fidelity. These results are similar to Schroeder's original findings [4] in terms of translational motion, however, the effect of yaw rotational motion was larger in every measured quantity. A mixed statistical analysis with measured data from the TU Delft and UTIAS experiments did not reduce the significance of the results of the current study.

The results from the capture task can be considered positive when used as a benchmark for the SRS simulator. The results showed comparable trends for all metrics, which is supported by the combined analysis of the TU Delft and UTIAS data. This is further supported by the similarities in the significance of the effects of sway motion when compared with the NASA and UTIAS studies. Also, the increased bandwidth and reduced delays of the SRS simulator showed positive trends in all of the metrics, although none were significant.

Analysis of the estimated parameters for identified pilot models in the different motion conditions indicated similar effects of translational and rotational motion: visual rate perception and neuromuscular stabilization strategies were reduced when either type of motion was added.

When replicating an experiment, technical characteristics of the apparatus can be matched well between facilities, provided that these characteristics are properly documented. However, human subjects will always remain a highly variable component in such comparisons. This study indicates that the human factor warrants at least as much attention as the purely technical aspects when designing these kinds of experiments.

Acknowledgments

The authors gratefully acknowledge the helicopter pilots who participated in this study, and would like to thank Peter R. Grant (University of Toronto Institute for Aerospace Studies, Toronto, Canada) for providing the visual database used in the experiments, and for providing the measurement data from his yaw capture experiment [5].

References

[1] Meiry, J. L., "Vestibular System and Human Dynamic Space Orientation," Ph.D. Thesis, Massachusetts Inst. of Technology, Cambridge, MA, 1965.

[2] Schroeder, J. A., "Simulation of Motion Effects on Single Axis Compensatory Tracking," *Proceedings of AIAA Flight Simulation Technologies Conference*, AIAA Paper 93-3579, Aug. 1993.

[3] Schroeder, J. A., "Evaluation of Simulation Motion Fidelity Criteria in the Vertical and Directional Axes," *Journal of the American Helicopter Society*, Vol. 41, April 1996, pp. 44–57.

[4] Schroeder, J. A., "Helicopter Flight Simulation Motion Platform Requirements," NASA, TR NASA/TP-1999-208766, Moffet Field, CA, July 1999.

[5] Grant, P. R., Yam, B., Hosman, R. J. A. W., and Schroeder, J. A., "Effect of Simulator Motion on Pilot Behavior and Perception," *Journal of Aircraft*, Vol. 43, No. 6, 2006, pp. 1914–1924. doi:10.2514/1.21900

[6] Groen, E. L., Smaili, M. H., and Hosman, R. J. A. W., "Perception Model Analysis of Flight Simulator Motion for a Decrab Maneuver," *Journal of Aircraft*, Vol. 44, March 2007, pp. 427–435. doi:10.2514/1.22872

[7] Hosman, R. J. A. W., Grant, P. R., and Schroeder, J. A., "Pre and Post Pilot Model Analysis Compared to Experimental Simulator Results," *Proceedings of AIAA Modeling and Simulation Technologies Conference*, AIAA Paper 2005-6303, Aug. 2005.

[8] Nieuwenhuizen, F. M., Zaal, P. M. T., Mulder, M., and Van Paassen, M. M., "New Multi-Channel Pilot Model Identification Method for Use in Assessment of Simulator Fidelity," *Proceedings of the AIAA Modeling and Simulation Technologies Conference and Exhibit*, AIAA Paper 2006-6629, 2006.

[9] Mah, R. W., and Young, L. R., "Thresholds for the Perception of Whole-Body Linear Sinusoidal Motion in the Horizontal Plane," AIAA Paper 1989-3273, 1989.

[10] Heerspink, H. M., Berkouwer, W. R., Stroosma, O., Van Paassen, M. M., Mulder, M., and Mulder, J. A., "Evaluation of Vestibular Thresholds for Motion Detection in the SIMONA Research Simulator," *Proceedings of the AIAA Modeling and Simulation Technologies Conference and Exhibit*, AIAA Paper 2005-6502, 2005.

[11] McRuer, D. T., and Jex, H. R., "Review of Quasi-Linear Pilot Models," *IEEE Transactions on Human Factors in Electronics*, Vol. HFE-8, No. 3, 1967, pp. 231–249.

[12] Van der Steen, H., "Self-Motion Perception," Ph.D. Thesis, Faculty of Aerospace Engineering, Delft Univ. of Technology, Delft, The Netherlands, 1998.

[13] Lean, D., and Gerlach, O. H., "AGARD Advisory Report No. 144: Dynamics Characteristics of Flight Simulator Motion Systems," AGARD, TR AR-144, 1979.

[14] Stroosma, O., Van Paassen, M. M., Mulder, M., and Postema, F., "Measuring Time Delays in Simulator Displays," *Proceedings of the AIAA Modeling and Simulation Technologies Conference and Exhibit*, AIAA Paper 2007-6562, 2007.

[15] Cooper, G. E., and Harper, R. P., "Use of Pilot Rating in the Evaluation of Aircraft Handling Qualities," NASA, TR TND-5153, 1969.
[16] Sinacori, J. B., "Determination of Some Requirements for a Helicopter Flight Research Simulation Facility," NASA, TR CR-152066, 1977.
[17] Mulder, M., "Cybernetics of Tunnel-in-the-Sky Displays", Ph.D. Dissertation, Faculty of Aerospace Engineering, Delft Univ. of Technology, Delft, The Netherlands, Nov. 1999.
[18] Hosman, R. J. A. W., "Pilot's Perception and Control of Aircraft Motions," Ph.D. Thesis, Faculty of Aerospace Engineering, Delft Univ. of Technology, Delft, The Netherlands, 1996.
[19] Groot, T., Damveld, H. J., Mulder, M., and Van Paassen, M. M., "Effects of Aeroelasticity on the Pilot's Psychomotor Behavior," *AIAA Atmospheric Flight Mechanics Conference and Exhibit*, AIAA Paper 2006-6494, Aug. 2006.
[20] Valente Pais, A. R., Mulder, M., Van Paassen, M. M., and Wentink, M., "Modeling Human Perceptual Thresholds in Self-Motion Perception," *Proceedings of the AIAA Modeling and Simulation Technologies Conference*, AIAA Paper 2006-6626, Aug. 2006.